Fluid dynamics of spacer filled rectangular and curvilinear channels

Ranade, Vivek V.; Kumar, Ashwani

Publisher's version / Version de l'éditeur:
https://doi.org/10.1016/j.memsci.2005.07.013
Journal of Membrane Science, 271, pp. 1-15, 2006

Available online at www.sciencedirect.com
SCIENCE DIRECT®
Journal of Membrane Science 271 (2006) 1–15
journal of MEMBRANE SCIENCE
www.elsevier.com/locate/memsci

Fluid dynamics of spacer filled rectangular and curvilinear channels☆

Vivek V. Ranade[a], Ashwani Kumar[b,*]

[a] Industrial Flow Modeling Group, National Chemical Laboratory, Pune 411008, India
[b] Institute for Chemical Process and Environmental Technology, National Research Council of Canada, M-12 Montreal Road, Ottawa, Ont., Canada K1A 0R6

Received 1 December 2004; received in revised form 5 July 2005; accepted 8 July 2005
Available online 22 August 2005

Abstract

Spacers are designed to generate significant secondary flow structures and create directional changes in the flow through membrane modules. Shape of the spacers used in membrane modules strongly influences the resulting flow and therefore performance of the module. In this work fluid dynamics of rectangular channels similar to membrane modules and containing different spacers was simulated using a three-dimensional computational fluid dynamics (CFD) model. A 'unit cell' approach was evaluated and used for this purpose. In addition to predicting the pressure drop, the simulated results provided significant insight into fluid dynamics of spacer filled channels. The validated CFD model was used to evaluate performance of different spacer shapes and understand the role of spacer shape and resulting fluid dynamics. The models were extended for the first time to simulate flow in spacer filled curvilinear channels, which could be useful in understanding the fluid behavior in spiral modules. The results were compared with those obtained with the flat channel. The approach and results presented in this work will have significant implications for identifying improved spacers with higher propensities to reduce fouling in membrane modules.

Keywords: Membrane modules; Spacers; CFD; Form drag; Viscous drag; Thin channels

1. Introduction

Pressure driven membrane processes are extensively used for pre-treatment, desalination and recycling in water and wastewater treatment industry. These processes usually suffer from concentration polarization and fouling caused by gradual build-up and deposit of dissolved and/or suspended species near and onto the surface of membranes. Some degree of fouling control can be achieved by the appropriate choice of operating parameters. Accumulation of rejected species can be suppressed by creating back mixing from the membrane to the bulk of the liquid. Sablani et al. [1] in a review on concentration polarization have commented on various techniques used to study and ease the problem. There is a need to design new products including spacers that are capable of alleviating the concentration build-up at a relatively lower pressure drop across the module. Spacers are introduced in membrane modules to separate membrane leaves and reduce fouling by modifying the fluid flow behavior. These spacers or turbulence promoters for spiral-wound and flat sheet modules are often net-like materials, which enhance mass transfer as well as provide passage for feed solutions. It is obvious that back mixing is more effective in spacer-filled channels than in empty channels. However, introduction of spacers also increases the pressure drop over the feed channel, i.e. the mechanical energy dissipation in the feed channel is higher in spacer-filled channels. Therefore, it is necessary to understand the role of spacer shape in resulting fluid dynamics of membrane modules. Such an understanding will allow optimization of spacer shapes to obtain an improved performance in terms of mass transfer and mechanical energy dissipation. An analysis by Da Costa et al. [2] of the processing costs in spacer filled channels, including equipment and energy consumption, demonstrated that there are distinct possibilities to optimize net spacers.

☆ NRCC no. 57853.

* Corresponding author. Tel.: +1 613 998 0498; fax: +1 613 991 2384.
E-mail addresses: vvranade@ifmg.ncl.res.in (V.V. Ranade), ashwani.kumar@nrc-cnrc.gc.ca (A. Kumar).

0376-7388/$ – see front matter © 2005 Elsevier B.V. All rights reserved.
doi:10.1016/j.memsci.2005.07.013

In recent years CFD techniques have been used by increasing number of researchers for understanding the fluid-flow behavior in membrane modules. Cao et al. [3] and Geraldes et al. [4] first reported two-dimensional CFD simulations of net and ladder type of spacers in narrow channels, respectively. These authors concluded that location and inter-filament distance of the spacers play an important role for shear stress distribution, mass transfer coefficients and pressure inside the channel. Karode and Kumar [5] reported studies on flow visualization and pressure drop estimation in spacers-filled channels. This work was probably the first attempt at using 3D CFD for modeling a thin channel with commercial spacers. These authors reported that bulk of the fluid does not change direction at each mesh as reported by Da Costa et al. [2,6]. It was also reported that pressure drops with symmetric spacers were higher than the asymmetric spacers, across an identical thin channel. Year 2002 saw a flurry of activity in the use of CFD techniques for studying spacers for membrane modules. Geraldes et al. [7] described a two-dimensional flow in rectangular channels filled with ladder-type spacers. They also reported 2D flow visualization and pressure drop. Schwinge et al. [8,9] reported two-dimensional CFD studies on hydrodynamics, mass transfer enhancement and estimation of foulant deposits in spacer filled channels. The flow characteristics were examined for arrangements of individual filaments in three different configurations namely zigzag, cavity and submerged with variation in mesh length and filament diameters. Li et al. [10,11] reported studies on optimizing the commercial net spacers for membrane modules using three-dimensional CFD simulations including the verification of their models with experimental data. These authors have shown the existence of transversal and longitudinal vortices, vortex shedding and instable flow behavior. Wiley and Fletcher [12,13] have made an attempt to apply CFD simulation for studying fluid dynamics of feed and permeate flows simultaneously. However, most of the reported work focused on 2D simulations. Many a time the grid independence of simulations was not clearly demonstrated. Furthermore, studies of fine flow structures in small independent cells and their impact on neighboring cells has not been reported in details. Recently, Koutsou et al. [14] reported a 2D flow simulation in a rectangular channel in the presence of cylindrical turbulence promoters similar to a case reported by Schwinge et al. [8,9]. They concluded that more realistic 3D simulations are needed for optimization of spacers. In a recent review, Schwinge et al. [15] described various experimental and computational techniques for understanding and improving the performance of spiral wound modules for various applications. They emphasized that CFD techniques should be used cautiously particularly considering complex processes, such as concentration polarization and solute rejection. Review of the previous work has shown that most workers have used CFD for very simple cases where selected filament configurations have been simulated in 2D. There is also a general lack of description of the computational procedures for CFD simulations including the selection of simulation parameters. Furthermore, published literature has mainly focused on rectangular channels with the assumption that this will be a good representation of the fluid flow behavior in spirals. The validity of this assumption needs to be verified. Therefore, there is a need for 3D simulations of commercial as well as new spacers in both rectangular and curvilinear channels.

In this work, we have evaluated and demonstrated the applicability of a 'unit cell' approach in understanding fluid dynamics of spacer filled channels. Detailed three-dimensional CFD models were developed to understand influence of spacer shapes on fluid dynamics of channels similar to membrane modules. For the first time, CFD simulations are reported for spacer filled curved channels, which would have direct relevance for spiral membrane modules. This study also reports the influence of radius of curvature, contributions of various drags and effects of spacer shapes on fluid dynamics. The approach and results presented in this work will have significant implications for identifying improved spacers with higher propensities to reduce fouling in membrane modules.

2. Computational model

2.1. Unit cell approach

Spacer-filled channels have stream wise periodic cross-sections. This means that the channel consists of a large number of identical cells. In a recent paper of Yuan et al. [16], it was shown that the flow and heat transfer in channels with stream wise-periodic cross-sections became 'periodic fully-developed' after a few cycles or cells. This finding is expected to apply also to the flow in channels with non-woven net spacers, which contains several hundreds of identical cells (see Fig. 1). Obviously, in a full size membrane module flow will be fully developed. Consideration of a unit cell offers possibility of resolving small-scale features of flow in greater detail without simulating the complete membrane module. This is especially important when one is interested in studying influence of spacer shapes on resulting fluid dynamics.

It is however essential to understand possible implications of approximating a spacer filled channel by periodic unit cells. It is well known that symmetry of a flow over a single cylinder breaks when Reynolds number increases beyond a critical Reynolds number of 60 [14]. The unit cell approach is not valid for cases where periodic symmetry of flow is absent despite the symmetric and periodic geometry. Fortunately, when cylinders are packed closely together in a regular fashion (as in spacer filled channels), the onset of symmetry breaking unsteady flow is delayed considerably. Hill et al. [17] have shown this for the case of spherical particles. Secondly in spacer filled channels, the fluid is increasingly confined and hence stabilized by neighboring spacers. For a specific Reynolds number, viscous dissipation will be higher at lower porosity, and therefore more effective in damping velocity fluctuations. Finally in spacer filled channels, cylin-

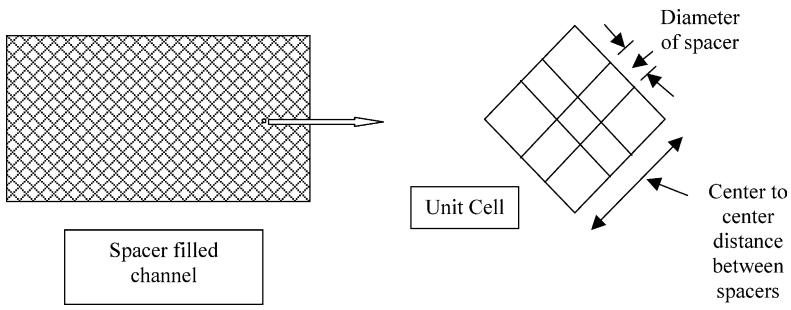

Fig. 1. Schematic of flat membrane module with spacer and unit cell.

ders are not perpendicular to the main flow direction. In fact flow gets aligned with the axis of the cylinders for most of the region. Moreover spacers always touch the channel walls. Considering these points, the symmetry breaking is unlikely in the spacer filled channels studied in this work. The unit cell approach was therefore used to understand influence of spacer shapes on fluid dynamics of spacer filled channels. Applicability of the 'unit cell' approach has also been discussed elsewhere in details [18,19].

2.2. Transition to turbulence in spacer filled channels

Flow in membrane modules is extremely complex and involves secondary flow structures and significant contribution of form drag. This flow is much closer to flow through packed beds rather than flow through channels. Similar to the packed beds, identification of a precise transition from laminar to turbulent flow regime in spacer filled channels is difficult as it occurs over a range of Reynolds numbers. The occurrence of transition to turbulence is a complex function of size and shape of spacers and packing characteristics. Previous studies on packed beds [20–23] indicate that transition occurs in the Reynolds number range of 300–400 (based on particle diameter). Unfortunately, there are no such reported studies on the transition to turbulence in spacer filled channels.

We have performed direct numerical simulations of flow through spacer filled channels with a commercial spacer using the 'unit cell' approach. Approximately one million computational cells were used to simulate flow in one unit cell of 0.02 cm^3 over a range of Reynolds numbers. At a Reynolds number of 350 (based on hydraulic diameter) and above, the simulations started capturing small scale flow features, which are signature of turbulence. It was interesting to note that when a steady state simulation under these conditions was attempted, a converged solution was not obtained. The steady state solution was possible when a turbulence model was used. This indicates that the flow instabilities are strongly related to small-scale turbulence rather than the asymmetric vortex shedding. This observation indirectly supports the conjecture that transition from laminar to turbulence in a spacer-filled channel occurs at the same Reynolds number range of 300–400 as reported for packed beds.

Though direct numerical simulations are in principle possible, these are prohibitively demanding on computational resources since unsteady flow simulations over a large period of time are needed to obtain statistically meaningful characteristics (e.g. pressure drop, strain rates and shear stress) of spacer filled channels. Turbulence models can be used instead to reduce computational demands. In this approach, small-scale (spatial and temporal) phenomena are not resolved but modeled using a 'turbulence model'. Several different turbulence models have been proposed [24]. The choice of an appropriate turbulence model is not straightforward. More complex model does not necessarily mean a better model. Often the simulated results have greater influence of the numerical issues (grid size and distribution, discretization schemes) than the differences in turbulence models. Since adequate information about turbulence characteristics of spacer filled channels was not available, we have used the standard k–ε model of turbulence following the literature recommendation [25]. Based on our direct numerical simulation results mentioned earlier and literature on transition to turbulence in packed beds, turbulence models were used for simulating flows above Reynolds number of 300. Cases with Reynolds number smaller than 300 were simulated using laminar flow model. Details of model equations and boundary conditions are discussed in the following section.

2.3. Model equations

Flow of a Newtonian fluid through a spacer filled channel was modeled by solving the Reynolds Averaged Navier Stokes (RANS) equations. The governing equations are listed below:

$$\frac{\partial}{\partial t}(\rho) + \nabla \cdot (\rho \bar{U}) = 0 \tag{1}$$

where t is the time, ρ the density of fluid and $\bar{U}$ is the time averaged fluid velocity.

$$\frac{\partial}{\partial t}(\rho \bar{U}) + \nabla \cdot (\rho \bar{U}\bar{U} + \rho \overline{uu}) = -\nabla \bar{p} - \nabla \cdot \bar{\tau} + \rho g \tag{2}$$

The over bar indicates a time-averaged value; u is a fluctuating velocity and p is pressure. τ is viscous stress tensor,

which is related to gradients of mean velocity as:

$$\tau_{ij} = \mu(\nabla \bar{U} + \nabla \bar{U}^{\mathrm{T}}) \tag{3}$$

where μ is coefficient of viscosity and the superscript 'T' denotes the transpose of a tensor quantity. In the present work, the viscosity and density of the process fluids were assumed to be constant.The Reynolds stresses (third term on left hand side of Eq. (2)) were modeled using an eddy viscosity concept as described elsewhere [26]:

$$-\overline{\rho u_i u_j} = \mu_{\mathrm{T}} \quad \frac{\partial \overline{U_i}}{\partial x_j} + \frac{\partial \overline{U_j}}{\partial x_i} \quad - \frac{2}{3}\delta_{ij} \quad \mu_{\mathrm{T}} \frac{\partial \overline{U_{\mathrm{k}}}}{\partial x_{\mathrm{k}}} + \rho k \tag{4}$$

Here, μ_{T} is turbulent or eddy viscosity, which in contrast to the molecular viscosity, is not a fluid property but depends on local state of flow or turbulence. It is assumed to be a scalar and may vary significantly within the flow domain. Turbulent kinetic energy, k, which is normal to turbulent stresses, can be expressed as:

$$k = \frac{1}{2}\overline{u_i u_i} \tag{5}$$

Substitution of Eqs. (3) and (4) in the Reynolds averaged momentum conservation equations (Eq. (2)) leads to a closed set, provided the turbulent viscosity is known. In this work, we used the standard k–ε model of turbulence. The turbulent viscosity is related to k and ε by the following reported equation [27]:

$$\mu_{\mathrm{T}} = \frac{C_\mu \rho k^2}{\varepsilon} \tag{6}$$

where C_μ is an empirical coefficient. The local values of k and ε can be obtained by solving their transport equations. The modeled form of transport equations of k and ε [27] can be written as:

$$\frac{\partial(\rho k)}{\partial t} + \frac{\partial(\rho U_i k)}{\partial x_i} = \frac{\partial}{\partial x_i} \quad \frac{\mu_{\mathrm{T}}}{\sigma_{\mathrm{k}}} \frac{\partial k}{\partial x_i} \quad + G - \rho\varepsilon \tag{7}$$

$$\frac{\partial(\rho \varepsilon)}{\partial t} + \frac{\partial(\rho U_i \varepsilon)}{\partial x_i} = \frac{\partial}{\partial x_i} \quad \frac{\mu_{\mathrm{T}}}{\sigma_\varepsilon} \frac{\partial \varepsilon}{\partial x_i} \quad + \frac{\varepsilon}{k}(C_1 G - C_2 \rho\varepsilon) \tag{8}$$

where G is the turbulence generation term given as:

$$G = \frac{1}{2}\mu_{\mathrm{T}} \ \nabla \bar{U} + (\nabla \bar{U})^{\mathrm{T}} \ ^2 \tag{9}$$

It can be seen that the standard k–ε model of turbulence uses five empirical parameters. The standard values of these parameters (i.e. C_{D}, C_1, C_2, σ_{k} and σ_ε were 0.09, 1.44, 1.92, 1.0 and 1.3, respectively) were used in the present work. It should be noted that the turbulence model was not used if Reynolds number was less than 350. In such cases, first three equations are adequate for simulations after setting turbulent stresses to zero. For cases with Reynolds number higher than 350, complete set of equations (Eqs. (1)–(9)) were solved. The details of solution domain and boundary conditions are discussed in the following section.

2.4. Solution domain, computational grid and boundary conditions

A periodic unit cell was considered as a solution domain. The geometry was modeled using the commercial grid generation tool, Gambit® (Fluent Inc., USA). The solution domain was divided into number of computational cells using Gambit®. Different numbers of cells were used to quantify the influence of grid size. The considered unit cell and solution domain for the case of Conwed-1 spacers are shown in Fig. 1.

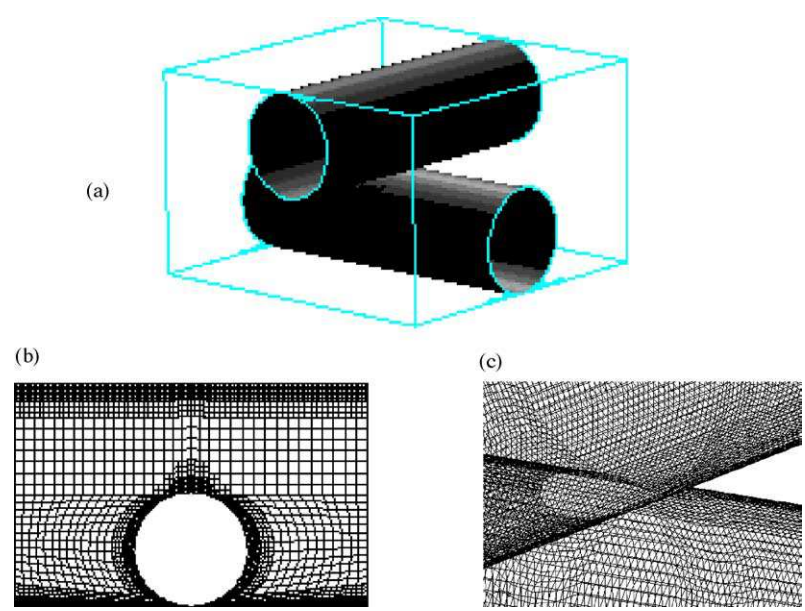

Fig. 2. Solution domain and computational grid for the flat channel filled with Conwed-1 spacer (a) solution domain, (b) face grid (c) close-up of intersection of spacers.

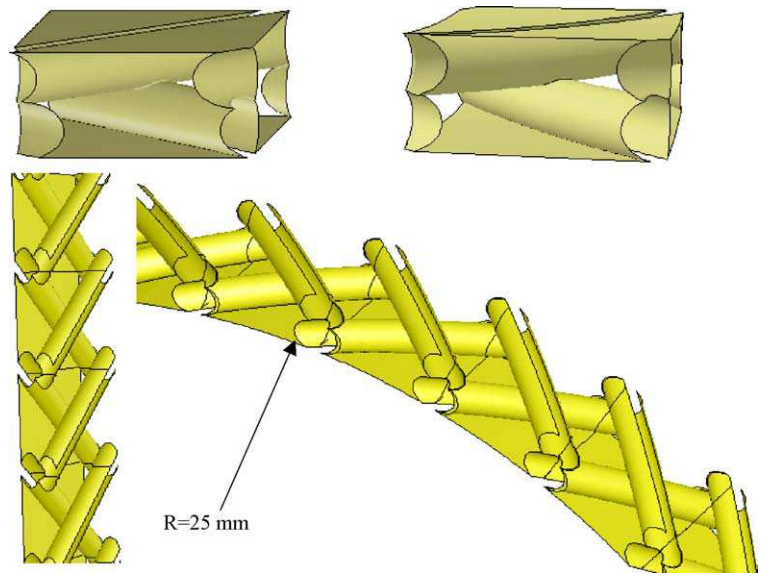

Fig. 3. Solution domain and computational grid for the curved channel filled with Conwed-1 spacer.

Center to center distance between the spacers was 3.2 mm. Therefore, the solution domain was considered as a rectangular block with dimensions of 3.2 mm × 3.2 mm × 2.01 mm. The cylindrical spacers were used with diameter of 1.03 mm. It can be seen that width of the channel is less than twice of spacer diameter and two spacers would intersect in order to fit in the channel. The close-up of such grids including intersection is shown in Fig. 2. Note that refined grids were used near all walls where steep gradients are expected. In addition to the Conwed-1 spacers, several other spacer shapes were computationally investigated. Simulations were also carried out with combination of two different spacers. The different spacers and configurations considered in the present work and their characteristic dimensions (hydraulic diameter and porosity) are listed in Table 1.

In spiral membrane modules, in addition to the direction changes created by spacers, the curvature of the channel affects the flow. The Dean vortices and other instabilities due to curvature are expected to enhance the performance of membrane modules [28]. The CFD models were therefore used to understand influence of curvature on flow in spacer filled channels. Flow simulations were carried out for spacer filled annular channels. Instead of spiral modules, channels were considered as annular. In order to establish procedures for geometry modeling and grid generation of spacer filled annular channels, a case of Conwed-1 spacers in an annulus of 50 mm inner diameter was considered. Following the 'unit cell' approach used in the flat channels, the geometry of annular 'unit cell' was modeled as shown in Fig. 3. Care was taken to ensure that the maximum skewness did not exceed 0.97. In fact, for the majority of the computational cells, the value of skewness was considerably less. For modeling the geometry of spacer filled annular channels, spacers of slightly larger size were used to avoid any gaps while building the geometry

Table 1
Characteristics of the spacers studied in this work

Configuration	Hydraulic diameter (m)	Porosity
Conwed-1	0.0015	0.741
Case-b	0.0010	0.765
Case-c	0.0014	0.709
Case-d	0.00092	0.679
Case-e	0.00103	0.665
Diamond	0.00160	0.811
Hexagon	0.00086	0.520
Case-f	0.00296	0.875
Case-b-with-holes	0.00106	0.789
CONWED-1-larger	0.00160	0.710
CONWED-1-spiral	0.00158	0.710
Case-b-spiral-25 mm radius	0.00163	0.607
Case-b-spiral-15 mm radius	0.00160	0.592
CONWED-1 with Case-b	0.00168	0.773

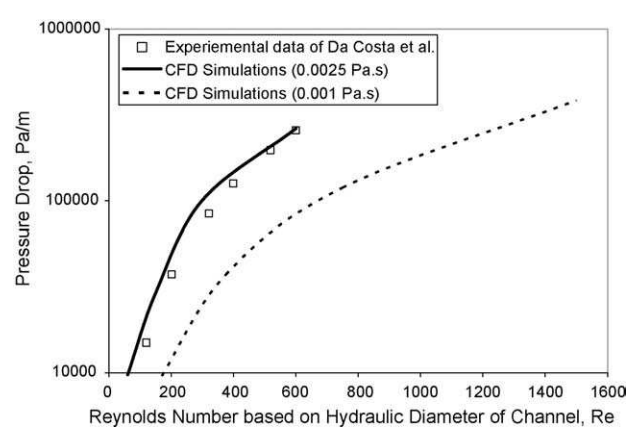

Fig. 4. Comparison of predicted results with experimental data of Ref. [2].

(for example, the diameter of Conwed-1 spacer was considered as 1.1 mm instead of 1.03 mm).

Vertical surfaces parallel to spacer cross-section were defined as translationally periodic boundaries with given mass flow rates. Pressure drop across the periodic faces was then iteratively adjusted to match the simulated flow rate with the set value of mass flow rate. Standard no-slip boundary conditions were specified at all walls. Several numerical experiments were carried out to understand influence of various parameters on predicted results. Key results of this study are discussed in the following section.

3. Results and discussion

It is essential to validate the developed computational model before applying it to understand the influence of spacer shapes on fluid dynamics of channels. Unfortunately, detailed flow measurements in spacer filled channels are difficult to perform and such experimental data is not available. However, Da Costa et al. [2] have reported overall pressure drop data for Conwed-1 spacers over a relevant range of superficial velocities. The CFD simulations of flow through channels with Conwed-1 spacers were therefore carried out for

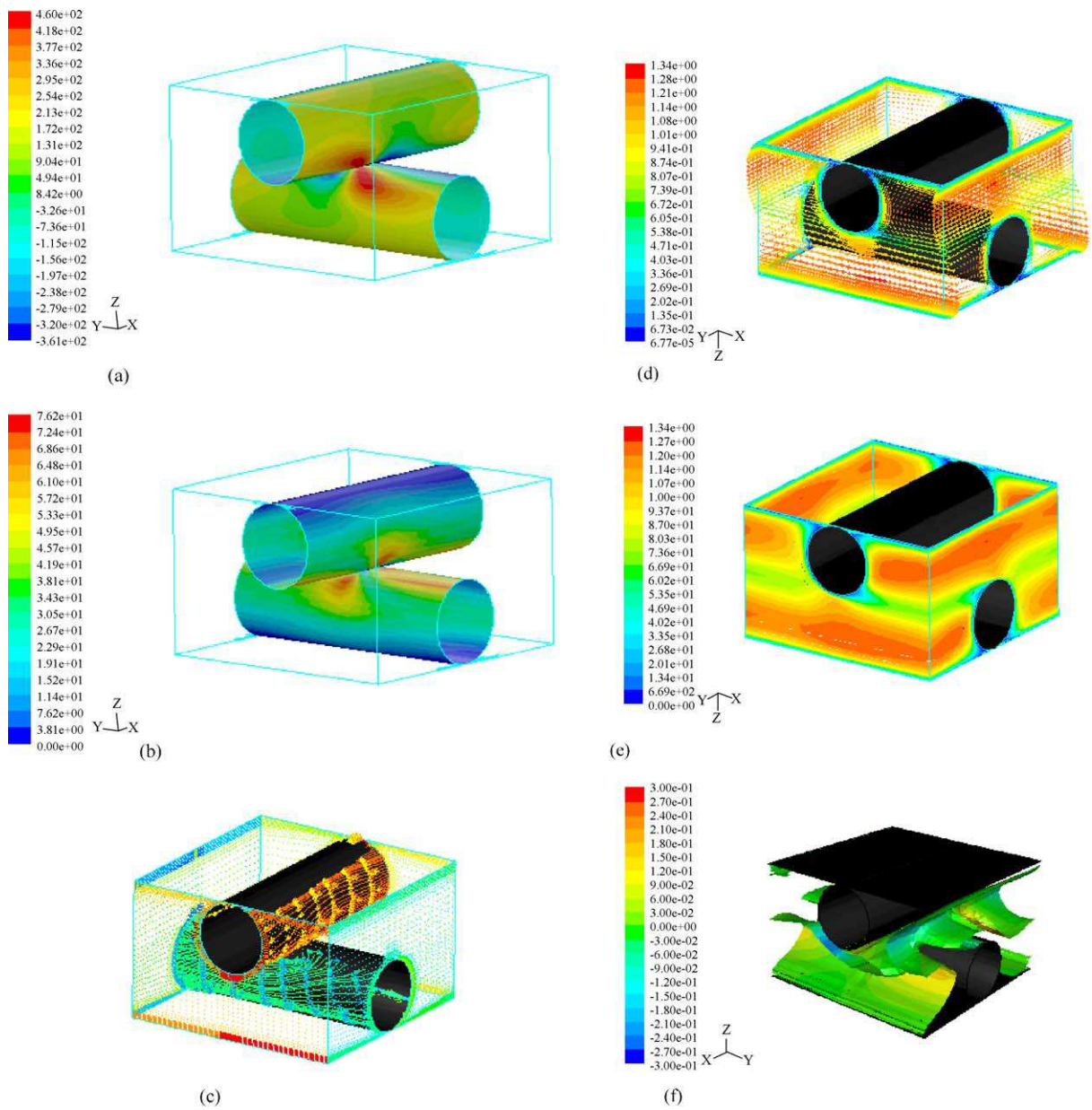

Fig. 5. Simulated results for the CONWED-1 spacer ($Re = 750$). (a) Contours of pressure on spacers (pressure, Pa). (b) Contours of wall shear stress on spacers (stress, Pa). (c) Path lines on spacers. (d) Transverse velocity field at periodic boundaries (velocity, m/s). (e) Contours of velocity magnitude at periodic boundaries (velocity, m/s). (f) Contours of z velocity on the surface of zero z-vorticity.

the range reported by Da Costa et al. [2]. Da Costa et al. performed their experiments with the Dextran solution. Following their earlier paper [29] the value of fluid viscosity in the simulations was specified as 0.0025 Pa s. With this viscosity and hydraulic diameter of about 1.5 mm, most of the experiments reported by Da Costa et al. [2,29] were below a Reynolds number of 350. Simulations of experiments of Da Costa et al. were therefore carried out with the laminar flow model.

Preliminary simulations were carried out to understand the influence of grid size and discretization schemes. These simulations indicate that if the number of computational cells used in the simulations is above 150,000, the predicted results are relatively insensitive to the actual number of cells used, provided second order discretization schemes were used. It will be useful to interpret the simulated results using the key dimensionless numbers. The flow in membrane modules is complex and is governed by different spatio-temporal scales. The choice of characteristic space and time scales are not always obvious. In the present work, we have followed the convention used in channel flows and have defined key dimensionless numbers based on hydraulic diameter and superficial velocity. Thus, the simulated results are interpreted by defining appropriate hydraulic diameter and the Reynolds number as:

$$Re = \frac{d_h V \rho}{\mu}; \quad d_h = \frac{4 \times \text{computational volume}}{\text{wet surface area}} \tag{10}$$

where V is superficial velocity. The predicted pressure drop values at different values of Reynolds number are compared with the data reported by Da Costa et al. [2] in Fig. 4. It can be seen that the predicted results agree with the experimental data reasonably well. The validated CFD model was then used to understand fluid dynamics of spacer filled channels.

3.1. Fluid dynamics of spacer filled channels

CFD model was used to simulate flow through spacer filled channels over a wide range of Reynolds numbers using the turbulence model. For all the subsequent simulations fluid viscosity was set to 0.001 Pa s. The values of predicted pressure drop for the range of Reynolds numbers with the Conwed-1 spacers are also shown in Fig. 4. It can be seen that in the laminar range, the pressure drop for the lower viscosity fluid (0.001 Pa s.) is almost six times lower than that for the higher viscosity fluid (0.0025 Pa s). This is expected since the pressure drop in the laminar range for a specific spacer configuration is proportional to the product of viscosity and superficial velocity. For example, at the same Reynolds number the superficial velocity for the higher viscosity fluid is 2.5 times that for the lower viscosity fluid leading to a pressure drop ratio of 6.25 for the two cases. As the Reynolds number increases above 300, linear relationship between Reynolds number and pressure drop is no longer valid (Fig. 4).

In addition to providing the pressure drop, the CFD simulations also provide detailed information about the fluid dynamics of spacer filled channels. To indicate the kind of information provided by the CFD simulations, typical results obtained for the Conwed-1 spacers (at Reynolds number of 750) are shown in Fig. 5. These results were obtained with 400,000 computational cells and with second order upwind differencing scheme. The contours of predicted pressure and shear stress on spacer surface are shown in Fig. 5a and b, respectively. It can be seen that high pressure and high shear stress zones exist near the region where fluid impacts on the spacers (i.e. near the cross-section of the spacers). The flow in the spacer filled channels is quite complex and involves significant changes in direction. In order to understand the directional flow changes due to spacers, the predicted path lines of mass less particles released on the periodic vertical surfaces are shown in Fig. 5c. To avoid clutter in this figure, only those path lines that are in the vicinity of surface of the spacers are shown. It can be seen that part of the tracer particle change direction at each cross-section though the significant portion of the flow gets aligned with the spacer direction. The alignment of the flow with the spacer direction can be clearly seen in Fig. 5d. The corresponding contours of velocity magnitude at the periodic boundaries are shown in Fig. 5e. The contours of axial velocity on a surface of z-vorticity of zero are shown in Fig. 5f. The surface of zero z-vorticity and contours of the axial velocity clearly indicate the regions with upward and downward motions and demonstrate the complex flow with several directional changes in the spacer-filled channels. It is difficult to bring out all the complexities of the flow in spacer-filled channels in static pictures. The state of the art computational flow visualization tools could be used to understand and visualize the detailed characteristics of fluid dynamics of spacer filled channels using the model presented here.

Overall pressure drop in a spacer filled channel is comprised of viscous drag on channel walls, viscous drag on spacers and form drag. It is important to understand the relative contributions of these different terms to gain an insight into influence of spacer shapes. Ideally spacers should be designed in such a way that it leads to minimum pressure drop

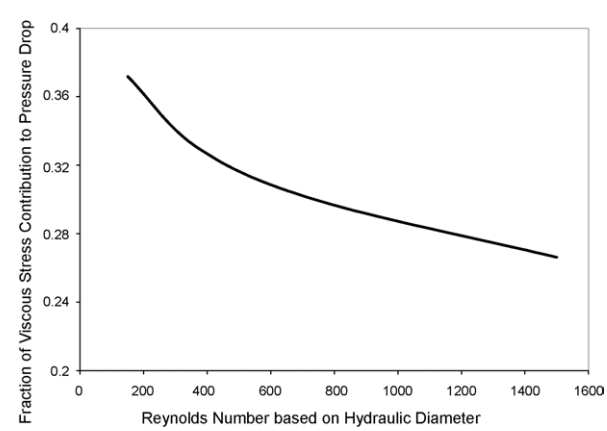

Fig. 6. Contributions of viscous stress to the overall pressure drop [Conwed-1 spacers].

with maximum strain rate. For constant viscosity fluids, this means, spacers should be designed to minimize form drag and losses due to directional changes. For a given pressure drop, a higher contribution of viscous drag, would lead to higher average strain rates near the wall. An experimental measurement of these contributions is very difficult. CFD models, however, provide such information conveniently. Simulated results were therefore analyzed to quantify different contributions to the overall pressure drop. Predicted local wall shear stress was averaged over wetted surface area (channel walls as well as spacers) to obtain contribution of the viscous stress. The predicted local pressure distribution around spacers was integrated to obtain form drag contribution in specified direction. There is no net pressure force acting on channel walls since the channel walls are parallel to the direction of flow. The predicted viscous stress contributions to the overall pressure drop for the Conwed-1 spacers for the range of Reynolds numbers are shown in Fig. 6. It can be seen that contribution of form drag to overall pressure drop is more than 60% for the Conwed-1 spacer. This fraction increases with increase

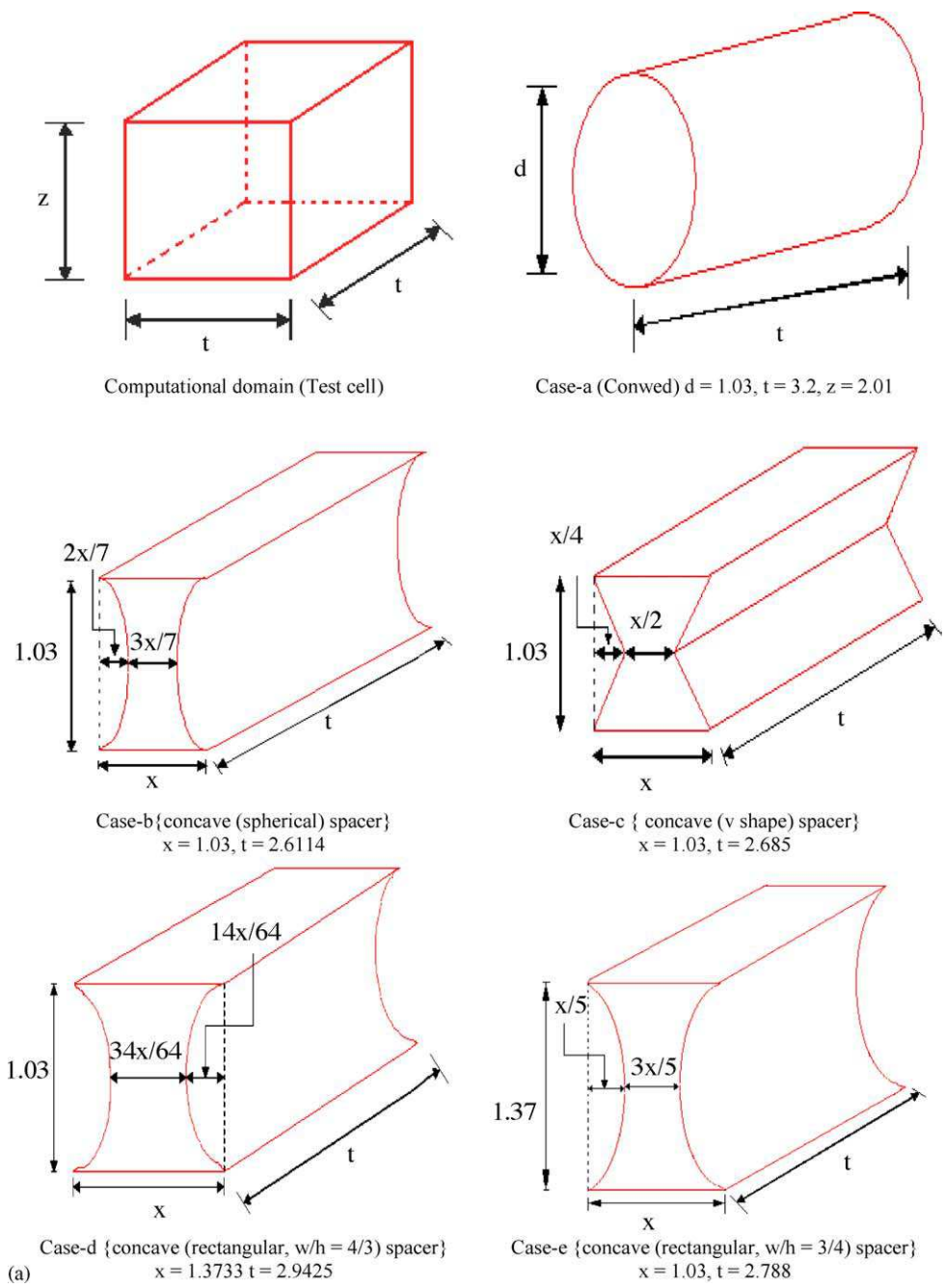

Fig. 7. (a) Geometry of considered flat channel and spacers proposed in Ref. [23]. (b) Additional geometry of considered flat channel and spacers proposed in this work.

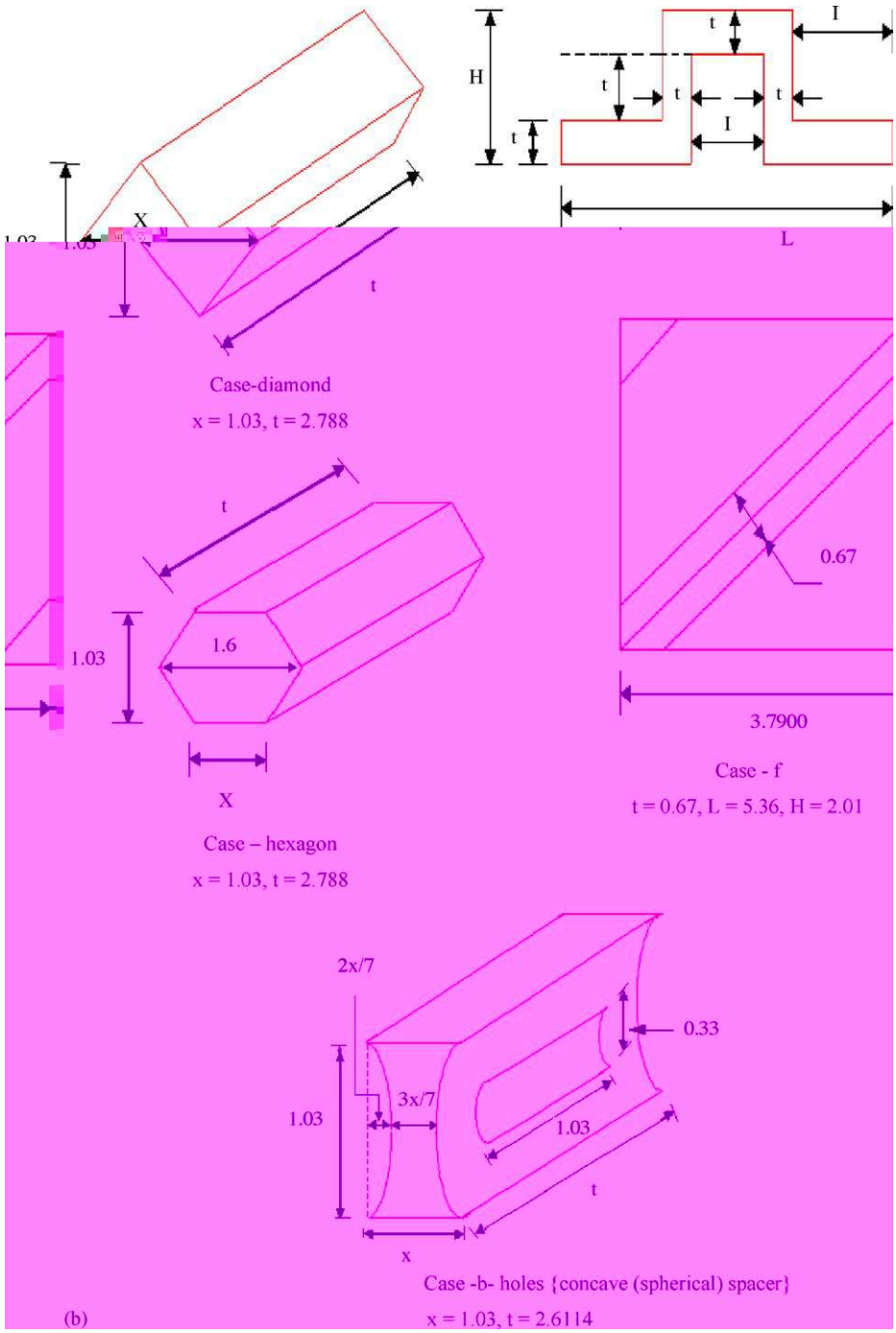

Fig. 7. (*Continued*).

in Reynolds number. Thus, more than half of input energy is not utilized to generate shear at the walls. New spacer shapes must be developed, which would minimize contribution of form drag to the overall pressure drop. Thus, motivation of developing new shapes is not only reduction of pressure drop but also to increase the relative contribution of viscous drag to the overall pressure drop. This will lead to better utilization of input energy.

3.2. *Influence of spacer shapes*

In order to reduce the form drag, spacers with different cross-sections like diamond or with concave surfaces were studied. Some spacers with holes or with just one-sided placement were also considered. The new shapes evaluated in this work are shown in Fig. 7a and b [30] (see Table 1 for characteristics of the spacer considered in this work). Flow

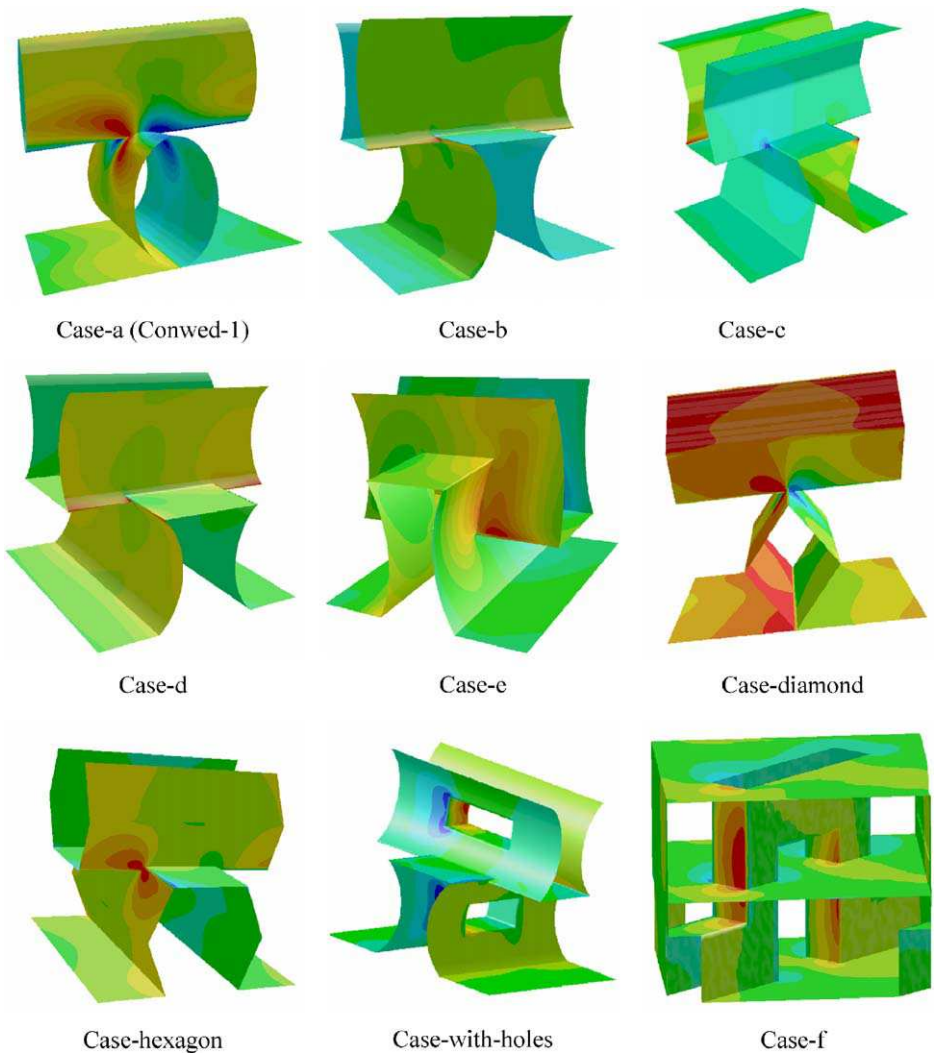

Fig. 8. Typical contours of predicted pressure drop for spacers of different shapes (Red, high; Blue, low). (For interpretation of the references to colour in this figure legend, the reader is referred to the web version of the article.)

simulations were carried out to understand the differences and similarities between fluid dynamics of these spacers. Typical contours of predicted pressure on selected spacers are shown in Fig. 8. It can be seen that spacer shapes and configuration have significant impact on the generated flow. It is perhaps not possible to discuss the simulated results of all the spacers in a single manuscript. However, the simulated flow characteristics of various spacers were analyzed in detail to understand the relative performance of different shapes. The analysis indicated the definite scope for optimization. As an example selected results of such an analysis are presented in the following paragraphs. Results of all the spacer shapes studies in this work are available from authors.

The predicted pressure drop values for some of the new spacers are compared with those of Conwed-1 in Fig. 9a. It can be seen that all the spacers shown in this figure exhibited pressure drop higher than the Conwed-1 spacer for the same Reynolds number (except may be the Case-c, which showed almost the same pressure drop as that of Conwed-1). It is interesting to examine these results in terms of dimensionless pressure drop or in terms of drag coefficient defined as:

$$C_{\mathrm{D}} = \frac{(\Delta P/L)d_{\mathrm{h}}}{(1/2)\rho U^2} \tag{11}$$

The results shown in Fig. 9a are presented in terms of drag coefficient in Fig. 9b. It can be seen that the spacers shown in Case-b and Case-d exhibit the lowest drag coefficients. The corresponding fraction of contribution of viscous stress in the overall pressure drop for these spacers is shown in Fig. 9c. It can be seen that in many cases the relative contribution of viscous stress to overall pressure drop is larger than that for the Conwed-1 spacer. This in fact leads to a possibility of optimization. The predicted area averaged values of wall shear stress for the different spacers are shown in Fig. 10a. It can be seen that most of the spacers shown in this figure were found to generate larger wall shear stress than the Conwed-1 spacer. It should be noted that the objective of identifying a new spacer shape is not just to reduce pressure drop or

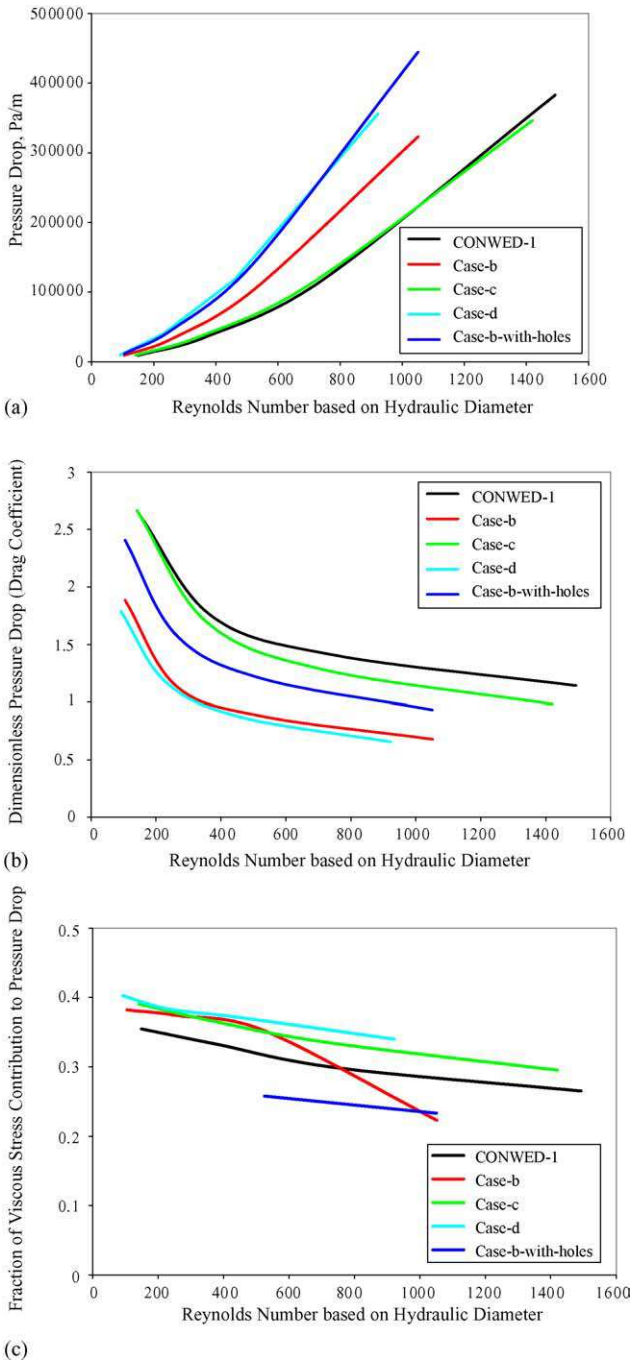

Fig. 9. Predicted results for selected spacers. (a) Predicted pressure drop. (b) Predicted drag coefficient. (c) Fraction of viscous stress contribution to overall pressure drop.

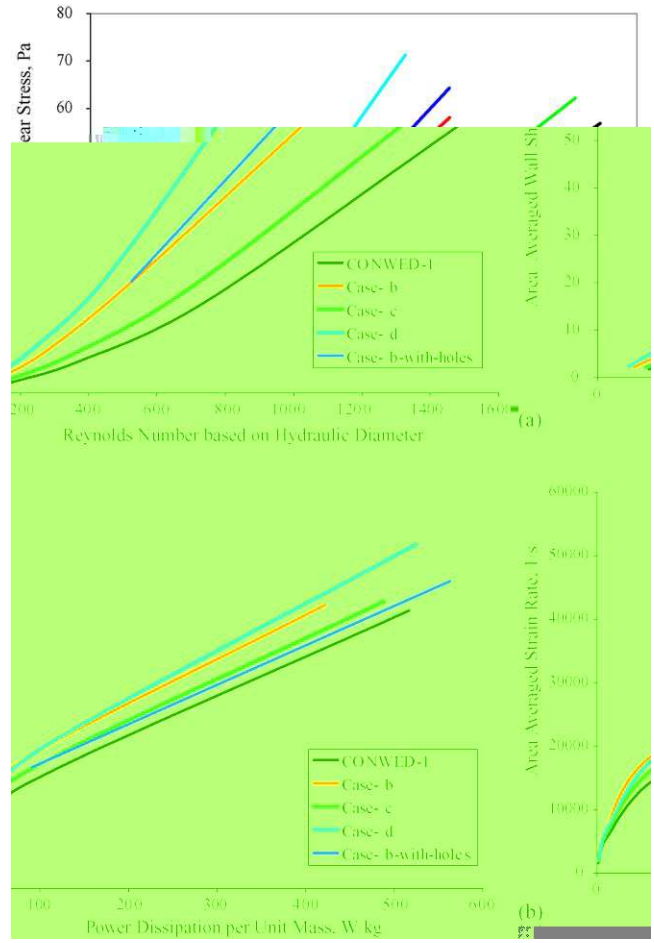

Fig. 10. Wall shear stress and strain rates of selected spacers. (a) Wall shear stress. (b) Average strain rates.

enhance wall shear rates but also to realize maximum wall shear rates per unit mass of energy dissipation rate. In order to examine the performance of different spacers from this perspective, the predicted area average values of wall shear rates are plotted as energy dissipation per unit mass (which was calculated as ratio of product of pressure drop per unit length and superficial velocity to the product of fluid density and porosity) in Fig. 10b. It can be seen that most of the spacers shown in this figure realize higher shear rates at the walls than Conwed-1 spacer for all energy dissipation rates. The spacers shown in Case-b and Case-d appear to be particularly promising amongst the considered configurations.

3.3. Flow through curved channels

Schock and Miquel [31] have shown that spacer-filled flat channels and channels in spiral wound modules with the same spacers exhibited similar flow characteristics. This means that pressure drops and mass transfer coefficients measured in flat channels are also valid for spiral wound modules. Available experimental data on comparison of flow in flat and curvilinear channels is rather scanty. It is indeed essential to thoroughly understand differences and similarities of flow in flat and curved channels for extending results obtained with flat channels to curved channels. In this work, we use CFD models for this purpose. The simulations can also provide significant insight into varying contributions of skin drag and form drag as the radius of curvature changes.

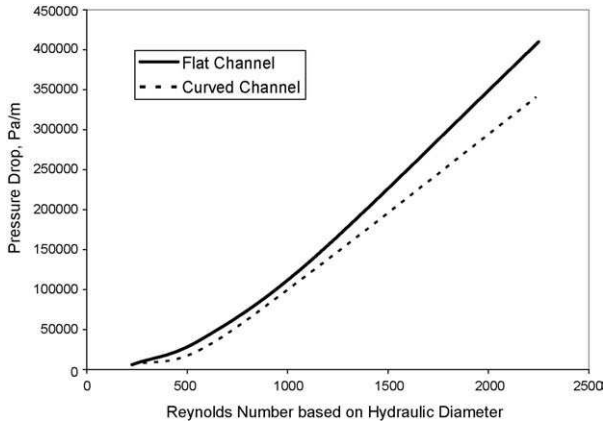

Fig. 11. Comparison of simulated pressure drop for flat and annular channels.

Flow in curved channels is more complex than that in flat channels due to the role of centrifugal force. The core fluid experiences a higher centrifugal force than the fluid near the outer wall. The fluid in the central part is driven towards the external wall by the centrifugal force. This causes a secondary flow, which moves the fluid near the wall inwards and the fluid near the center outwards. Thus, the characteristics of flow through an empty flat channel and an empty curved channel are drastically different. However, unlike the empty channel, significant secondary flow structures exist in the spacer filled flat channels. The secondary flows caused by the curvature are therefore expected to be of much lesser consequence as compared to those in empty channels. This was investigated numerically using a unit cell approach.

For making consistent comparisons, similar spacer geometry in a flat channel was also simulated. It may be noted that unstructured tetrahedral grids were used in these simulations (Fig. 3). Influence of discretization grids and number of computational cells was also examined. It was observed that the predicted results are not very sensitive to the discretization scheme when number of computational cells exceeded 180,000. For example, in a flat channel, the difference between simulated pressure drop with first and second order upwind discretization scheme with 188,245 cells was within 1.2% for superficial velocity of 1 m/s. Flow in annular channels was simulated for about 190,000 and 540,000 computational cells for superficial velocity of 0.1 m/s. The difference in the predicted pressure drop was within 1.2%. Difference in the predicted pressure drop between 190,000 and 540,000 cell simulations may increase with increase in superficial velocity. However, for the present work 190,000 cell simulations were found to be adequate. All of the subsequent simulations were based on 190,000 cells and second order differencing scheme.

The simulated results for the spacer (Conwed-1) filled flat and annular channels were analyzed in detail to understand the differences and similarities of the flow characteristics. The predicted values of pressure drop per unit length for the flat and curved channels are shown in Fig. 11. It may be noted that unlike the relative pressure drops of curved and straight pipes, the simulated values of pressure drop for annular channels were lower than those obtained for the flat channels. The difference is however not very significant (especially for Reynolds number up to 1200) and might have been caused by small changes in the dimensions of flat and annular channels. The observation is not surprising because, unlike in the case of straight and curved pipes, the secondary flow structures are always present in the case of the spacer filled channels. The predicted flow fields at the mid-plane parallel to membrane surfaces are shown in Fig. 12 for the flat and the curved channels. It can be seen that predicted flow field in flat and curved channels appear almost the same. This conclusion is further reinforced by the comparison of predicted wall shear stress and vorticity (not shown here). It may be instructive to make quantitative comparison of predicted flow field at some locations. Such comparison of velocity magnitude along a line passing mid-way through the side faces of the solution domain is shown in Fig. 13. It can be seen that the predicted velocities in flat and curved channel are quite similar. It is interesting to note the asymmetry in the predicted profiles for the curved channels. The predicted velocity values for the fluid stream passing near the outer curved surface was found to be higher than that passing near the inner curved surface. This is similar to the observations made for the curved channel flows without the spacers.

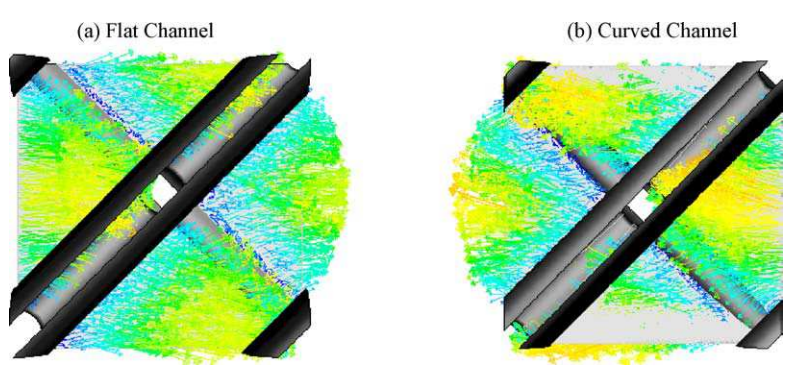

Fig. 12. Velocity field at mid-plane parallel to membrane surfaces (Red, maximum velocity, Blue, zero velocity). (For interpretation of the references to colour in this figure legend, the reader is referred to the web version of the article.)

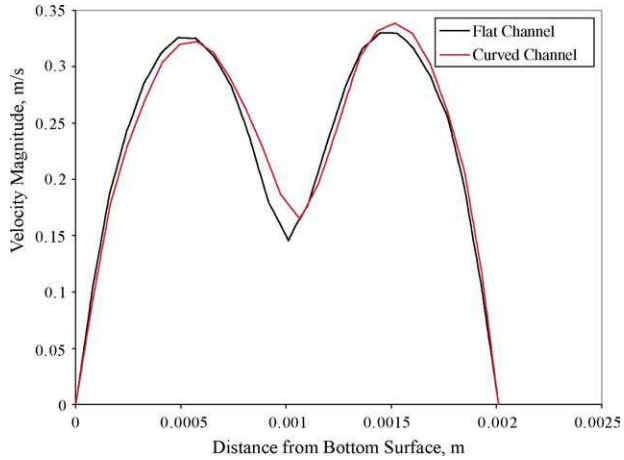

Fig. 13. Comparison of predicted velocity profile for flat and curved channels.

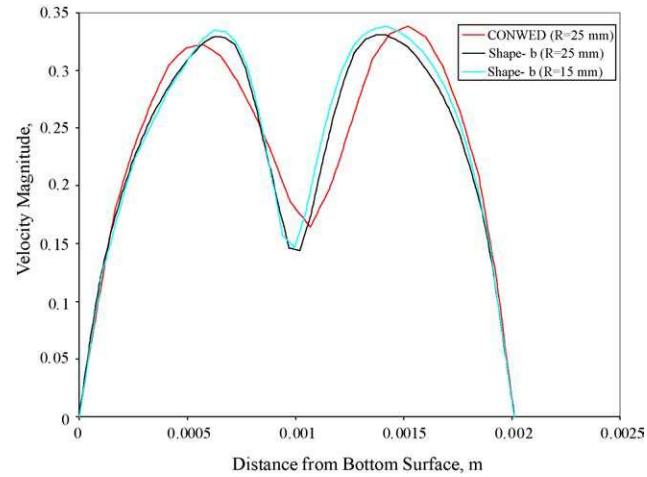

Fig. 14. Influence of spacer shape and radius of curvature on predicted flow.

The predicted results obtained for the flat and curved channels clearly indicate that for spacer filled channels there is no significant difference in the flow field. Unlike the empty channels, for the spacer filled channels, curvature is not essential for realizing the secondary flows. Secondary flows are present even in the absence of the curvature. Secondly, since the channel size is small, the values of dimensionless curvature (for low values of distance between spacers, dimensionless

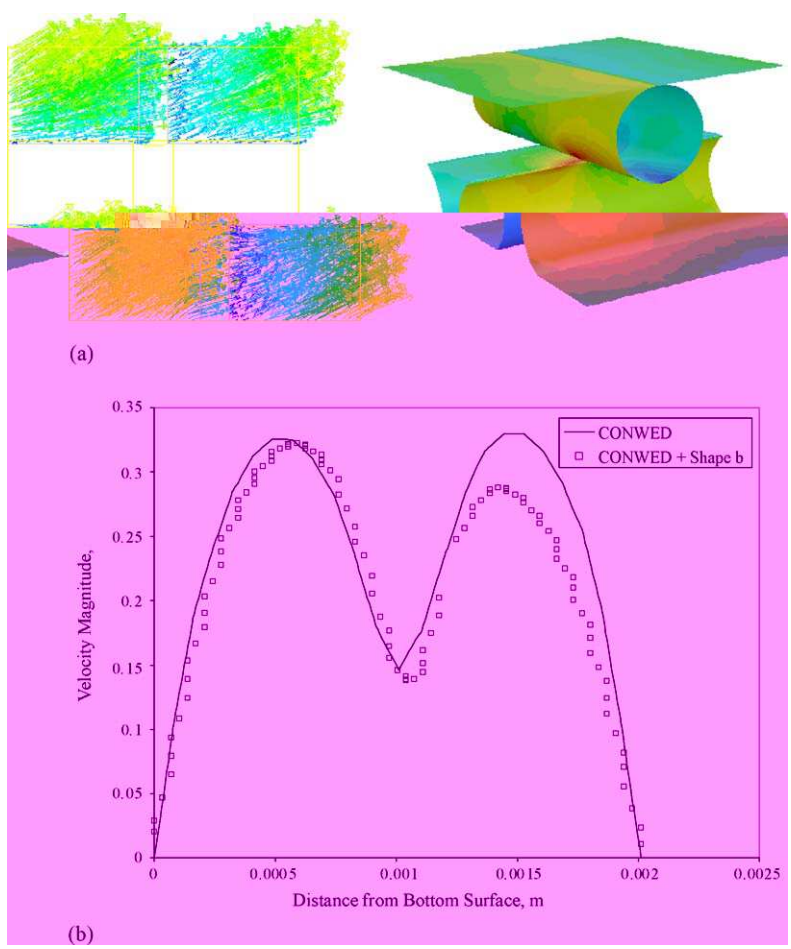

Fig. 15. Predicted results for the combination of spacers CONWED-1 and Case-b. (a) Velocity vectors and pressure contours (Red, high; Blue, low). (b) Comparison of predicted velocity profiles. (For interpretation of the references to colour in this figure legend, the reader is referred to the web version of the article.)

curvature can be approximated as a ratio of hydraulic diameter and annulus diameter) were less than 0.05 for the cases considered here. Thus, the secondary flows created by the spacers are much stronger than those influenced by such low values of curvature. The simulations therefore support the conclusion of Schock and Miquel [30] about the similarity of spacer-filled flat channels and spiral channels. This means that pressure drops and mass transfer coefficients measured in flat channels may provide adequate guidelines, which are also valid for spiral wound modules.

In order to understand the influence of spacer shape on flow field, flow through curved channels with Shape-b spacers was simulated for different superficial velocities with two different curved channels. Quantitative comparison of the predicted velocity profiles for Conwed-1 and Case-b is shown in Fig. 14. It can be seen that though spacer shape influence the flow in spacer filled channels significantly, the radius of curvature has no significant influence on the generated flow. This indirectly confirms that the secondary structures formed in spacer filled channels are dominated by the spacer configurations and are not significantly affected by the curvature of the channels.

3.4. Use of CFD model to evaluate new ideas

Several different spacer shapes were investigated during the course of this work. An interesting variation of ideas on spacer shape is possibility of using two different strands in a variety of combination. As an example, a case of combination spacer made of Conwed-1 strand and a Case-b strand (which was found to be more efficient among the new shapes) was investigated. Since the curvature of the channel was not found to affect the flow characteristics significantly, the study was carried out using a flat channel. The predicted flow field as vector plots and contours of pressure are shown in Fig. 15a. The quantitative comparison of predicted velocity profiles for standard Conwed-1 spacers and a combination spacer is shown in Fig. 15b. It can be seen that the presence of Shape-b filament does not significantly affect the velocity profile in the region dominated by Conwed-1 spacers. The velocity magnitude of the other half relevant to Shape-b is slightly different than the Conwed-1 side. The pressure drop for the combination spacers is less than that observed for the Conwed-1 spacers. For example, for a superficial velocity of 0.1 m/s, pressure drop for the combination spacers is 4700 Pa/m as against 6300 Pa/m for the Conwed-1 spacers. The idea of different combinations of spacers and spacer shapes appears to be promising. The computational approach, models and results demonstrate the power and potential of computer simulations to provide detailed information about the relationship between spacer shapes and resulting fluid dynamics and its possible influence on membrane performance. The approach and models presented here can be used to evaluate new ideas on spacer shapes and their combinations for applications to membrane modules.

4. Conclusions

The following conclusions were drawn from this study:

1. Significantly large number of computational cells was needed to capture influence of spacer shape on resulting fluid dynamics of membrane modules. It is therefore very difficult to carry out detailed 3D simulations of a full membrane module. However, a 'unit cell' approach can be used successfully.
2. Considering the closely packed spacers in a membrane module unsteady flow characteristics, which usually occur in flow over bluff bodies, were damped.
3. Contributions of form drag and viscous drag to the overall pressure drop could be quantified by a CFD model.
4. Fluid dynamics of spacer filled flat and curved channels was not significantly different. Results obtained with flat modules could therefore be used to estimate performances of spiral wound membrane modules with spacers.
5. Shapes of spacer strands influence the fluid flow behavior significantly. Our simulations have shown that spacer strands with 'shape b' reduce the pressure drop significantly while strain rate values were reasonable. This spacer shape appears to be optimal among the investigated shapes.
6. The idea of partial modifications of spacer by changing the shape of only one of the strand appears to be promising.

Acknowledgement

Authors are grateful for the financial support provided by Middle East Desalination Research Center (MRDRC) for this work under the project 00-BS-005.

Nomenclature

C_1	parameter of the standard k–ε model (Eq. (8))
C_2	parameter of the standard k–ε model (Eq. (8))
C_μ	parameter of the standard k–ε model (Eq. (6))
C_D	drag coefficient (Eq. (11))
d	spacer diameter
d_h	hydraulic diameter of spacer filled channel
g	gravitational acceleration
G	turbulence generation rate
k	turbulent kinetic energy
$\bar{p}$	mean pressure
ΔP	pressure drop
Re	Reynolds number (defined by Eq. (10))
t	time or dimension defined in Fig. 7a
u	fluctuating velocity
$\bar{U}$	time averaged fluid velocity
V	superficial velocity

x	dimension defined in Fig. 7a or spatial co-ordinate
z	dimension defined in Fig. 7a

Greek letters

ε	turbulent energy dissipation rate
μ	viscosity
μ_T	turbulent viscosity
ρ	density
σ_k	turbulent Prandtl number of turbulence kinetic energy
σ	turbulent Prandtl number of turbulence energy dissipation rate
τ	shear stress

References

[1] S.S. Sablani, M.F.A. Goosen, R. Al-Belushi, M. Wilf, Concentration polarization in ultrafiltration and reverse osmosis: a critical review, Desalination 141 (2001) 269–289.

[2] A.R. Da Costa, A.G. Fane, D.E. Wiley, Spacer characterization and pressure drop modeling in spacer-filled channels for ultrafiltration, J. Membr. Sci. 87 (1994) 79–98.

[3] Z. Cao, D.E. Wiley, A.G. Fane, CFD simulations of net-type turbulence promoters in a narrow channel, J. Membr. Sci. 185 (2001) 157–176.

[4] V. Geraldes, V. Semião, M.N. de Pinho, Mass transfer experiments and CFD modeling for spacer-filled slits with semi-permeable membrane walls, in: Luque, S., Alvarez, J. (Eds.), Proceedings of Engineering with Membranes, Granada, Spain, June 2001, pp. 210–215.

[5] S.K. Karode, A. Kumar, Flow visualization through spacer filled channels by computational fluid dynamics-I: pressure drop and shear rate calculations for flat sheet geometry, J. Membr. Sci. 193 (2001) 69–84.

[6] A.R. Da Costa, A.G. Fane, C.J.D. Fell, A.C.M. Franken, Optimal channel spacer design for ultrafiltration, J. Membr. Sci. 62 (1991) 275–291.

[7] V. Geraldes, V. Semião, M.N. de Pinho, Flow management in nanofiltration spiral wound modules with ladder-type spacers, J. Membr. Sci. 203 (2002) 87–102.

[8] J. Schiwinge, D.E. Wiley, D.F. Fletcher, Simulation of the flow around spacer filaments between narrow channel walls. 1. Hydrodynamics, Ind. Eng. Chem. Res. 41 (2002) 2977–2987.

[9] J. Schiwinge, D.E. Wiley, D.F. Fletcher, Simulation of the flow around spacer filaments between narrow channel walls. 2. Mass-transfer enhancement, Ind. Eng. Chem. Res. 41 (2002) 4879–4888.

[10] F. Li, A.B. de Haan, T. Reith, Study of flow patterns for mass transfer enhancements by spacers in spiral wound module by CFD simulation, in: Proceedings of Engineering with Membranes, Granada, Spain, 2001.

[11] F. Li, W. Meindersma, A.B. de Haan, T. Reith, Optimization of commercial net spacers in spiral wound membrane modules, J. Membr. Sci. 208 (2002) 289–302.

[12] D.E. Wiley, D.F. Fletcher, Computational fluid dynamics modeling of flow and permeation for pressure-driven membrane processes, Desalination 145 (2002) 183–186.

[13] D.E. Wiley, D.F. Fletcher, Techniques for computational fluid dynamics modeling of flow in membrane channels, J. Membr. Sci. 211 (2003) 127–137.

[14] C.P. Koutsou, S.G. Yiantsios, A.J. Karabelas, Numerical simulation of the flow in plane channel containing a periodic array of cylindrical turbulence promoters, J. Membr. Sci. 231 (2004) 81–90.

[15] J. Schwinge, P.R. Neal, D.E. Wiley, D.F. Fletcher, A.G. Fane, Spiral wound modules and spacers: review and analysis, J. Membr. Sci. 242 (2004) 129–153.

[16] Z.X. Yuan, W.Q. Tao, Q.W. Wang, Numerical prediction for laminar forced convection heat transfer in parallel plate channels with stream wise periodic rod disturbances, Int. J. Numer. Methods Fluids 28 (1998) 1371–1387.

[17] R.J. Hill, D.L. Koch, A.J.C. Ladd, Moderate-Reynolds-number flows in ordered and random arrays of spheres, J. Fluid Mech. 448 (2001) 243–278.

[18] P.R. Gunjal, V.V. Ranade, R.V. Chaudhari, Computational study of single-phase flow in packed bed of spheres, AIChE J. 51 (2005) 365–378.

[19] G.E. Karniadakis, B.B. Mikic, A.T. Patera, Minimum-dissipation transport enhancement by flow destabilization: Reynolds' analogy revisted, J. Fluid Mech. 192 (1988) 365–391.

[20] M.A. Latifi, N. Midoux, A. Storck, J.N. Gence, The use of microelectrodes in the study of flow regimes in a packed bed reactor with single phase liquid flow, Chem. Eng. Sci. 44 (1989) 2501–2508.

[21] D. Seguin, A. Montillet, J. Comiti, Experimental characterization of flow regimes in various porous media. I. Limit of laminar flow regime, Chem. Eng. Sci. 53 (21) (1998) 3751–3761.

[22] D. Seguin, A. Montillet, J. Comiti, F. Huet, Experimental characterization of flow regimes in various porous media. II. Transition to turbulent regime, Chem. Eng. Sci. 53 (22) (1998) 3897–3909.

[23] Rajendra P. Chhabra, Jacques. Comit, Ivan. Machac, Flow of non-Newtonian fluids in fixed and fluidised beds, Chem. Eng. Sci. 56 (2001) 1–27.

[24] D.C. Wilcox, Turbulence Modeling for CFD, DCW Industries Inc., La Canada, California, USA, 1993.

[25] V.V. Ranade, Computational Flow Modeling for Chemical Reactor Engineering, Academic Press, London, UK, 2002.

[26] B.E. Launder, D.B. Spalding, The numerical calculations of turbulent flows, Comput. Methods Appl. Mech. Eng. 3 (1974) 269–289.

[27] B.E. Launder, D.B. Spalding, Lectures in Mathematical Modeling of Turbulence, Academic Press, London, UK, 1972.

[28] N. Al-Bastaki, A. Abbas, Use of fluid instabilities to enhance membrane performance: a review, Desalination 136 (2001) 255–262.

[29] A.R. Da Costa, A.G. Fane, C.J.D. Fell, A.C.M. Franken, Optimal channel spacer design for ultrafiltration, J. Membr. Sci. 62 (1991) 275–291.

[30] D. Dendukuri, S.K. Karode, A. Kumar, Flow visualization through spacer filled channels by computational fluid dynamics. II. Improved feed spacer designs, J. Membr. Sci. 249 (2005) 41–49.

[31] G. Schock, A. Miquel, Mass transfer and pressure loss in spiral wound modules, Desalination 64 (1987) 339–352.